Electrochemical reduction and protonation of a biomimetic diiron azadithiolate hexacarbonyl complex: Mechanistic insights

Marc Bourrez, Frédéric Gloaguen

https://doi.org/10.1016/j.bioelechem.2023.108488

Electrochemical reduction and protonation of a biomimetic diiron azadithiolate hexacarbonyl complex: mechanistic insights

Marc Bourrez, Frederic Gloaguen

CNRS, Univ Brest, CEMCA UMR 6521, 6 av Le Gorgeu, F-29238 Brest, France

frederic.gloaguen@univ-brest.fr

Abstract

The electrochemical reduction and protonation of $[Fe_2(adt^H)(CO)_6]$ (**1**, $adt^H = SCH_2N(H)CH_2S$) and $[Fe_2(pdt)(CO)_6]$ (**2**, $pdt = SCH_2CH_2CH_2S$) in the presence of moderately strong acid in acetonitrile was investigated by cyclic voltammetry (CV), focusing on the catalysis of hydrogen evolution reaction (HER) by a $\{2e^-,2H^+\}$ pathway. The turnover frequencies at zero overpotential (TOF_0) of the N-protonated product **1**$(H)^+$ and **2** for the HER were estimated from simulations of the catalytic CV responses at low acid concentration using a simple ECEC mechanism (two electrochemical and chemical steps). This approach confirmed that **1**$(H)^+$ is clearly a better catalyst than **2**, pointing to a possible role of the protonable and biologically relevant adt^H ligand in the enhancement of the catalytic performances. Density functional theory (DFT) calculations further suggested that, owing to a strong structural rearrangement in the course of the catalytic cycle, the HER catalysis by **1**$(H)^+$ only involves the iron center adjacent to the amine group in adt^H and not the two iron centers as in **2**. Since terminal hydride species (FeFe–H) are known to more easily undergo protonolyse to H_2 than their bridging hydride isomers (Fe–H–Fe), this may explain here the enhanced activity of **1**$(H)^+$ over **2** for the HER.

1. Introduction

It has long been known that some microorganisms produce molecular hydrogen (H_2) in the course of their normal metabolism. Over the last three decades, the structural characterization and a better understanding of the functions of the underlying enzymes, called [NiFe]- and [FeFe]-hydrogenases (H_2ases),[1,2] have paved the way for the design of biomimetic catalysts for the hydrogen evolution reaction (HER).[3][4][5][6][7] Crystallographic and spectroscopic studies have revealed that one of the key features of the active site of [FeFe]-H_2ases is an unprecedented azadithiolate (adt^H) bridging ligand (Scheme 1).[8] It has been further proposed that the amine group in adt^H is well suited to shuttle protons to and from the adjacent iron center facilitating thus the heterolytic formation and

activation of H_2. Several studies have demonstrated that transition metal complexes bearing "adt-type" bridging ligands are indeed among the most efficient biomimetic HER catalysts and could even activate H_2 oxidation.[9–12] Importantly, it has also been reported that employing a bioinspired outer coordination sphere in combination with an "adt-type" second coordination sphere can help promote reversible H_2 production and uptake by mononuclear Ni catalysts.[13]

To evaluate the proton shuttling function of adt^H in biomimetic diiron complexes, we previously compared the catalytic activity for the HER in acetonitrile (MeCN) of the azadithiolate complex $[Fe_2(adt^H)(CO)_6]$ (**1**) with that of a structurally related propanedithiolate (pdt) complex $[Fe_2(pdt)(CO)_6]$ (**2**) lacking that functionality (Scheme 1).[14–16] Assuming, for both HER catalysts, a simple $E_{rev}C_{cat}$ mechanism (E_{rev} stands for a fast electrochemical step and C_{cat} for an irreversible bimolecular catalytic step with a bimolecular rate constant k_{cat}) and using the corresponding foot-of-the-wave analysis (FOWA, see below) of the cyclic voltammetry (CV) response, we found that the intrinsic activity of **1** is at least two orders of magnitude larger than that of **2**, independently of the strength of the acid used as a proton source ($8.0 < pK_a^{MeCN} < 15.0$). By analogy with the proposed biocatalytic mechanism, we thus suggested that the enhanced activity of **1** arises from the proton shuttling function of the amine group in adt^H. Density functional theory (DFT) calculations allowed us to further infer that the electrochemical reduction of the N-protonated product $\mathbf{1}(H)^+$ triggers a subsequent tautomerization step leading to an iron-hydride intermediate. This assumption has been recently challenged by the results of a study of the reactivity of **1** towards protons by time-resolved UV-vis and IR spectroscopy.[17] In particular, IR stopped flow experiments showed that the chemically reduced N-protonated intermediate **1**(H) slowly decays to a product which spectra can be assigned to **1** or an iron-hydride species. This observation suggests that in any case the tautomerization step should be slow, ruling out this mechanism to explain the enhanced catalytic activity of **1**. The proposed alternative is that the reaction of **1**(H) with acid to give a bridging hydride occurs at a faster rate because it involves a lower structural reorganization than with the corresponding reduced pdt intermediate $\mathbf{2}^-$. On the other hand, a detailed CV study has shown that the HER catalysis associated with the reduction of **2** is limited by the slow release of H_2 from the $\{2e^-,2H^+\}$ intermediate, not by the first protonation step.[18] Similarly, another CV study has established that the HER catalysis by the adt^R complex $[Fe_2(adt^R)(CO)_6]$ (R = C_2H_4OMe, **3**) entails two different catalytic mechanisms, the first one taking place at the reduction potential of the N-protonated product $\mathbf{3}(H)^+$ and being also limited by the slow release of H_2.[19]

Key metrics to benchmark the activity of homogeneous catalysts for the activation of an electrochemical reaction can be derived from the overpotential for catalysis η_{cat} and the turnover frequency TOF.[20] The overpotential for catalysis is defined as the difference between the redox

potential ($E_{1/2}$) of the active form of the catalyst and the reversible potential ($E^0_{substrate}$) of the electrochemical reaction ($\eta_{cat} < 0$ for a reduction). The turnover frequency can be estimated from current enhancement i_{cat}/i_p, where i_p is the CV peak current associated with the reduction or the oxidation of the catalyst in the absence of substrate and i_{cat} the height of the catalytic wave. However, this approach provides reliable results only under specific conditions that are not always experimentally achievable. As a result, Savéant and coworkers developed the FOWA method in the framework of the CV response for a two steps $E_{rev}C_{cat}$ mechanism occurring under a "pure kinetic" regime mixed with "side-phenomena", such as substrate depletion or catalysts deactivation.[21] With this method, the value of the bimolecular catalytic rate constant k_{cat} is directly calculated from the slope of the linear portion of a plot of i/i_p vs. $1/(1 + \exp(F(E - E_{1/2})/RT))$. Then, the variation of TOF = $k_{cat}[substrate]_{bulk}$ with the driving force $\eta = E - E^0_{substrate}$ gives access to a so-called "catalytic Tafel plot" from which the intrinsic turnover frequency TOF_0 at zero driving force can be extracted. As discussed above, we previously estimated the activity of **1** and **2** for the HER in MeCN using this original form of FOWA (i.e. assuming an $E_{rev}C_{cat}$ mechanism). The method has since been refined to take into account more general catalytic scenarios, i.e. EECC, ECEC or ECCE mechanisms.[22] FOWA is now extensively employed to benchmark homogeneous catalysts for various electrochemical reactions. However, recent CV simulation studies have demonstrated that the use of FOWA in the case of multi-electron multi-step catalytic reactions operating far from a "pure kinetic" regime could lead to erroneous values of TOF and hence of TOF_0.[23,24]

In parallel with electrochemical and spectroscopic methods, computational chemistry methods are more and more employed to help analyzing experimental data and to decipher the mechanisms of homogeneous catalysis of electrochemical reactions. In this context, DFT calculations have proved particularly useful to determine the structure and estimate acidity constant and redox potential of catalytic intermediates, and thus to establish structure/function relationships.[25–28]

In light of the recently published works questioning the role of adt^H as proton relay in the HER catalysis by **1** and the degree of applicability of the FOWA method to estimate its intrinsic catalytic activity, we decided to carry out a complementary mechanistic study of the reactivity of this biomimetic complex using CV simulations and DFT calculations. Herein, we report on the thermodynamics and kinetics of the reduction and protonation of **1** at low concentrations of moderately strong toluenesulfonic acid (HOTs, $8.0 \leq pK_a^{MeCN} \leq 8.6$). Then, comparisons with the reactivity of the pdt derivative **2** and previously studied adt^R analogue **3** are established with the objective of deciphering whether or not subtle differences between dithiolate bridging ligands have major mechanistic implications.

2. Experimental

2.1. Chemicals

$[Fe_2(adt^H)(CO)_6]$ (**1**) and $[Fe_2(pdt)(CO)_6]$ (**2**) were available from previous studies.[15] Tetrabutylammonium hexafluorophosphate (Bu_4NPF_6) from Sigma-Aldrich was purified by crystallization in methanol. HPLC-grade acetonitrile (MeCN) and *p*-toluenesulfonic acid monohydrate (HOTs) from Sigma-Aldrich were used as received.

2.2. Electrochemistry

The cyclic voltammetry (CV) experiments were carried out in a 10 mL one-compartment glass cell (Metrohm) using a µ-Autolab potentiostat and the GPES software. The electrolyte, a solution of 0.1 M Bu_4NPF_6 in MeCN, was purged by N_2. The working electrode, a glassy carbon (GC) electrode (Metrohm) of 0.071 cm^2 in surface area, was carefully polished with alumina paste prior to all experiments. The counter electrode was a tungsten wire. Special attention was placed on minimization of the ohmic drop by using diluted solutions of diiron dithiolate hexacarbonyl compounds (≤ 0.5 mM) and by placing the tip of the calomel reference electrode (Tacussel) compartment as close as possible to the GC disk used as working electrode. The uncompensated solution resistance was $R_u \approx 130\ \Omega$. The proton source concentration was varied by addition of small volumes of 0.2 M HOTs solution in MeCN. Ferrocene (Fc) was added as an internal reference at the end of each experiment. All potentials in this paper are referenced to that of the oxidation of Fc. All CV peak potentials and currents were measured after background current subtraction using QSoas (version 3.1).[29][30]

CV simulations were carried out with home-made software adapted from CVSIM.[31] The objective of the simulations was not to reproduce the complete CV response under catalytic conditions, but rather to possibly obtain better estimates of the TOF values than those previously calculated using FOWA. Consequently, the diffusion coefficient was set to $D = 10^{-5}$ cm^2 s^{-1} for all species and the heterogeneous rate constant and symmetry coefficient values were set to $k_h = 0.2$ cm s^{-1} and $\alpha = 0.5$ for all redox processes.

2.3. Electronic structure calculations

The Cartesian inputs for DFT calculations were prepared with Avogadro (version 1.20).[32] The DFT calculations were performed at the B3LYP-D3/def2-TZVP level of theory using ORCA (version 5.03).[33–36] The calculations were accelerated with the resolution of identity and chain of sphere (RIJCOSX) approximations in combination with a suitable auxiliary basis set (def2/J).[37] The geometries were optimized without structural constraints in the gas phase. The vibrational frequencies were calculated analytically without scaling factor and analyzed to confirm that the optimized geometries are located at a stationary point and to calculate the thermochemical

contributions at 298.15 K. Single point calculations were carried out on the optimized geometries using the SMD solvation module to take into account the effect of MeCN (ε = 35.688).[38] The standard potentials (E^0) vs. SCE and the acidity constants (pK_a) in MeCN were calculated following well-established procedures.[39] The calculated standard potentials were converted to the Fc scale by adding −0.38 V.[40]. The pictures of the structures were generated by CYLView (version 1.0b).[41] the Fukui functions were calculated using Multiwfn (version 3.8).[42,43]

3. Results and discussion

*3.1. Electrochemical reduction of **1** in the absence of a proton source*

The first diffusion limited electrochemical reduction of **1** in Bu_4NPF_6/MeCN takes place at $E_{1/2}$ = −1.58 V (Fig. 1A), a reduction potential close to that of **3** ($E_{1/2}$ = −1.56 V) and **2** ($E_{1/2}$ = −1.60 V),[44] emphasizing that the nature of the bridgehead group (NH, NC_2H_4OMe or CH_2, Scheme 1) of the bridging ligand has little effect on the level of the LUMO of this series of complexes. In the case of aryl amine substituted diiron hexacarbonyl complexes, a noticeable effect of the nature of aryl group on the reduction potential has in contrast been reported.[45] At slow scan rates, the pair of CV peaks associated with the reduction of **1** exhibits of a peak-to-peak separation of $\Delta E_p \approx 65$ mV, a value comparable to that measured for the fast one-electron oxidation of Fc under similar experimental conditions (i.e. no ohmic drop compensation). A peak current ratio $i_{p,a}/i_{p,c} < 1$ and the presence of several oxidation peaks on the reverse scan are nevertheless the signs of a follow-up chemical reaction. As shown in Fig. 1B, the normalized reduction peak current $-i_{p,red}\, v^{-1/2}\, [\mathbf{1}]^{-1}$ slightly increases when the scan rate decreases from v = 12 to 0.1 V s^{-1}, which can be ascribed to the scan rate dependent effect of the follow-up chemical reaction on the CV response. Accordingly, the reduction of **1** involves only one electron even on the longer CV timescales.

The electrochemical reduction of the pdt derivative **2** and the adt^R analogue **3** has been previously described in great details.[18,44] These complexes show both a transition from a one to two-electron reduction at slow scan rates, at odds with what is observed here for **1**. In the case of **3**, the transition is attributed to a fast disproportionation of the anion $\mathbf{3}^-$, a process apparently not favored with **1**.

*3.2. Electronic structures of **1** and its reduced forms*

To try to address the above issue, we calculated by DFT the electronic structures of **1** and its one and two-electron reduced derivatives $\mathbf{1}^-$ and $\mathbf{1}^{2-}$. The optimized geometry of the neutral form **1** is in excellent agreement with experiment (Table 1), in particular the length of the Fe–Fe (2.51 Å) and Fe–S (2.29 Å) bonds, which are the most altered upon electron transfer (see below). An inspection of the potential energy surface (PES) of the reduced forms $\mathbf{1}^-$ and $\mathbf{1}^{2-}$ reveals for each redox state two minima, in which either the butterfly structure of **1** is retained (isomer **A**) or one Fe–S bond is

cleaved and one CO ligand is in a bridging position (isomer **B**) (Fig. 2). Similar structures have previously been calculated for the one and two-electron reduced derivatives of **3**.[44] At the anionic state $\mathbf{1}^{-}$, the difference in free energy in solution indicates that isomer **A** is ca. 55.5 kJ mol^{-1} more stable than isomer **B**, ruling out the occurrence of a large structural rearrangement upon the first electron transfer. This finding is consistent with the recent analysis of $\mathbf{1}^{-}$ by UV-vis and IR spectroscopy.[17] We note however a significant elongation of the Fe–Fe distance (2.87 Å), confirming that the first electron transfer populates the σ*(Fe–Fe) orbital. At the dianionic state $\mathbf{1}^{2-}$, isomer **A** is still about 13.1 kJ mol^{-1} more stable than isomer **B**, suggesting that the cleavage of the Fe–S bond is again not favored upon a second electron transfer. By contrast, isomer **B** was found significantly more stable than isomer **A** in the two-electron reduced derivative $\mathbf{3}^{2-}$ (albeit in the gas phase).[44] This discrepancy might explain why potential inversion driven by a Fe–S bond cleavage, and thus an overall two-electron reduction on longer CV timescales, is not favored in the biologically-relevant derivative **1**. This finding is further supported by the DFT calculations of the standard reduction potentials $E^0(\mathbf{1}/\mathbf{1}^{-}) = -1.54$ V and $E^0(\mathbf{1}^{-}/\mathbf{1}^{2-}) = -2.39$ V. Note that the value calculated for $E^0(\mathbf{1}/\mathbf{1}^{-})$ is close to the experimental value (–1.58 V) and 0.04 V less negative than that calculated for $E^0(\mathbf{2}/\mathbf{2}^{-})$ again in good agreement with the experiment ($\Delta E_{1/2} = 0.02$ V).

*3.3. Electrochemistry of **1** and **2** in the presence of toluenesulfonic acid*

Fig. 1C shows the CVs of **1** in the presence of increasing concentrations of HOTs ($8.0 \le pK_a^{MeCN} \le 8.6$). At low acid concentrations (4 molar equivalents), the HER catalysis occurs at about –1.3 V, a potential close to the estimated reduction potential of the N-protonated product $\mathbf{1}(H)^{+}$. The catalytic current at this potential does not further increase with the acid concentration suggesting a catalytic process limited by the slow release of H_2. At higher acid concentrations (12 molar equivalents), the catalytic wave still increases in height but exhibits a shoulder at ca. –1.30 V while its peak potential shifts to more negative values (< –1.40 V) indicating the occurrence of a new acid responsive process. This second catalytic process will not be further discussed in the following because it likely entails $\{3e^{-},3H^{+}\}$ pathways that are less relevant to decipher the role of adt^{H} in the reactivity of **1** towards protons. Similarly, a second catalytic process occurring at more negative potentials, and involving hence more than two electrons and protons, has been reported for the pdt derivative **2** and the adt^{R} analogue **3**.[18,19]

Fig 1D shows that, in the case of **1** and contrary to **2**, the peak current enhancement $i_{cat}/i_{p,red}$ at low acid concentration slightly decreases as the scan rate v increases from 0.1 to 2 V s^{-1}. This behavior can be explained by a CE process. In the vicinity of the electrode, the protonation equilibrium between $\mathbf{1} + H^{+}$ and the N-protonated form $\mathbf{1}(H)^{+}$ (C step) is displaced towards the formation of the

latter because its reduction (E step) occurs at a less negative potential than that of **1**.[15] Accordingly, we evaluated the catalytic activity for the HER at slow scan rate (v = 0.1 V s^{-1}), when the formation of **1**(H)$^+$ at the electrode is comparatively fast and therefore not rate limiting.

It has been well established that the HER catalysis by **2** in the presence of moderately strong acid, such as HOTs in MeCN, follows an ECEC mechanism.[18] According to previous reported data on the adt^R analogue **3**,[19] the experimental data described above and the DFT calculations described below, we have also chosen to simulate the catalytic CV responses of **1** in the presence of 4 molar equivalents of acid with a ECEC mechanism (Scheme 2). We further consider that the N-protonated product **1**(H)$^+$ is the active form of the catalyst formed at the electrode by a comparatively fast CE process (see above). This CE process is simulated by adding a fast irreversible C step of rate constant of 10^6 M^{-1} s^{-1} before the first E step of the ECEC mechanism (Scheme 2). The catalytic cycles are then similar for both **1**H$^+$ and **2**. The first E step at E^0_1 is followed by a fast bimolecular C step of rate constant k_1, a second E step at $E^0_2 > E^0_1$ and finally a rate limiting bimolecular C step of rate constant k_2 leading to evolution of H_2 and recovery of the active form of the catalyst. Importantly, it has been shown that for an ECEC mechanism where $E^0_2 > E^0_1$ and $k_2/k_1 << 1$, as it is the case here, FOWA cannot not provide a value for k_2 and therefore for TOF = k_2[substrate] and TOF_0 (see below).[20,24]

The values of the parameters E^0_1, E^0_2, k_1 and k_2 used to simulate the catalytic CV responses of **1**H$^+$ and **2** are listed in Scheme 2. In both cases, the rate constant of the C step following the first E step was set to $k_1 = 10^6$ M^{-1} s^{-1} and the potential of the second reduction step to $E^0_2 = E^0_1 + 0.05$ V. The values of E^0_1 and k_2 were then adjusted to fit the peak potential and current enhancement $i_{cat}/i_{p,red}$ of the experimental catalytic CV response (Fig. 3). The values of E^0_1 derived from CV simulations are in fair agreement with the experimental value of the reduction peak potential of **1**(H)$^+$ ($E_{p,c}$ = −1.27 V, Fig. 1)[15] and in very good agreement with the experimental value of the reduction potential of **2** ($E_{1/2}$ = −1.60 V).[44] The best fit values of k_2 give values of TOF = $k_2[H^+]$ = 1.2 and 3.2 s^{-1} for **1**(H)$^+$ and **2**. The TOF value for **1**(H)$^+$ is of the same order of magnitude to that previously calculated for **3**(H)$^+$ (TOF = 3 ±0.5 s^{-1}).[19] In addition, the TOF value calculated here for **2** is in good agreement with the previously reported value derived also from CV simulations.[18]

The reversible potential of the couple HOTs/H_2 in MeCN depends on the pK_a of the acid and on the reversible potential of the H^+/H_2 couple, for which there is a disagreement between the reported values.[20,46] Here, we used E^0_{HOTs} = −0.65 V, which gives values of overpotential for catalysis $\eta_{cat} = E^0_1 - E^0_{HOTs}$ = −0.66 and −0.95 V for **1**(H)$^+$ and **2**. From that, we calculated the values of the intrinsic turnover frequency at zero driving force $TOF_0 = TOF \exp(F(E^0_1 - E^0_{HOTs})/RT) \approx 8 \times 10^{-12}$ and 3×10^{-16}

s^{-1} for **1**$(H)^+$ and **2**. This result confirms that **1**$(H)^+$ is several orders of magnitude more efficient than **2** when the HER catalysis follows a $\{2e^-,2H^+\}$ pathway.

*3.4. Electronic structures of the reduced and protonated forms of **1** and **2***

To further validate our DFT calculations, we first computed the acid/base and redox properties of **1** and **1**$(H)^+$ in MeCN. The calculated pK_a value (8.5) of the amine function in **1** is close to the experimental value (8.0 ±0.2) and the calculated reduction potential value (−1.15 V) of the N-protonated product **1**$(H)^+$ is slightly less negative than that derived from CV simulation (−1.31 V).

Fig. 4 shows the most likely pathway calculated by DFT for the HER catalysis by **1**$(H)^+$. As expected, the N-protonation of **1** to form **1**$(H)^+$ has negligible effect on the structure of the Fe_2S_2 core: the optimized length of the Fe−Fe bond is 2.52 Å (Fig. 4). The protonated reduced intermediate **1**(H) adopts a structure very similar to that calculated for the isomer **A** of $\mathbf{1}^-$ with an elongated Fe−Fe distance (2.91 Å) and no Fe−S bond cleavage. This result suggests that the reduction of **1**$(H)^+$ is a simple one-electron process that does not involve any potential inversion. The next step must be the formation of an iron-hydride intermediate **1**$(H,H)^+$, which is a key precursor in the formation of H_2 activated by diiron complexes. We evaluated two different pathways that may lead to an iron-hydride. First, an internal proton transfer (i.e. a tautomerization) from the N-protonated bridgehead to the adjacent iron site gives a terminal hydride.[15] This process, uphill by ca. 3.0 kJ mol^{-1}, is followed by a N-protonation step (pK_a = 9.4). Second, the direct protonation of the diiron bond (pK_a = 9.2) gives a bridging-hydride. Our calculations indicate that the structure of **1**$(H,H)^+$ in which the hydride is in bridging position is slightly more stable (−1.9 kJ mol^{-1}) than that with a terminal hydride, so we favor the second pathway over the first one. The optimized structure of **1**$(H,H)^+$ shown in Fig. 4 is also more consistent with the conclusions derived from the recent spectroscopic study of the reactivity of **1** towards protons.[17] The reduction of **1**$(H,H)^+$ at a calculated reduction potential of −1.30 V induces a large structural rearrangement of the catalyst. In **1**(H,H), the Fe−Fe distance (3.43 Å) is strongly elongated and the $Fe(CO)_3$ moiety adjacent to the amine group of adt^H is rotated opening a vacant site on the corresponding iron center. Finally, the strongly exergonic reaction of **1**(H,H) with H^+ (−179.5 kJ mol^{-1}) releases H_2 and regenerates **1**$(H)^+$. Note that this final step also implies that NH_2^+ in **1**$(H)^+$ is formed from the hydride ligand in **1**(H,H), which could be favored by the large structural rearrangement and the low basicity of the $Fe(CO)_3$ moiety.

Catalysis of the HER by the pdt derivative **2** in the presence of moderately strong acid such as HOTs is known to proceed through the protonation of a bridging hydride intermediate (Fe−H−Fe).[47,48] On the other hand, detailed spectroscopic and electrochemical studies on phosphine-substituted diiron dithiolate complexes have revealed that the presence of adt^H favors the formation of terminal

hydride species (FeFe–H) that are reduced at milder potentials and more easily undergo protonolyse to H_2 than their isomeric bridging hydride counterparts.[8] Accordingly, we reasoned that a possible explanation for the enhanced catalytic activity of **1**(H)$^+$ over **2** could be the involvement of a terminal hydride rather than a bridging hydride intermediate in the catalytic cycle. To support this hypothesis, we calculated the Fukui function for an electrophilic reaction (i.e. protonation) in **1**, **2** and their reduced protonated forms involved in the HER catalysis (Fig. 5). As expected, the reactive sites for protonation are in between the two-iron center in **1** and **2** and on the nitrogen atom of adt^H in **1**. In the case of the one-electron reduced intermediates **1**(H) and **2**$^–$, the reactive sites for protonation are again in between the two-iron center favoring thus the formation of a bridging hydride intermediate, which is consistent with our DFT calculations described above (Fig. 4). The reactive sites for protonation of the two-electron intermediate **2**(H)$^–$ remain in between the two iron centers and the bridging hydride, confirming that H_2 is released by protonation at this position. The situation is completely different in the two-electron intermediate **1**(H,H). The gain in electron density is mostly located on the iron center adjacent to the amine group in adt^H and on the nitrogen atom. The other iron center bearing the hydride exhibits no noticeable gain or loss of electron density, which means that it will not be directly involved in the formation of H_2. This result provides strong support to the assumption that the HER catalytic mechanism with **1**(H)$^+$ involves a terminal rather than a bridging hydride intermediate, explaining its enhanced catalytic activity compared to **2**.

4. Conclusions

The main objective of this study was to evaluate the catalytic activity of the N-protonated product **1(**H)$^+$ and the structurally related pdt derivative **2** for the HER in acetonitrile using the moderately strong toluenesulfonic acid as a proton source. We speculated that, at low acid concentrations, when the catalytic cycle follows a {2e$^–$,2H$^+$} pathway, the protonable and biologically relevant adt^H ligand may play a role in the catalytic mechanism. Simulations of the catalytic CV responses using a simple ECEC mechanism allowed us to calculate the turnover frequency at zero overpotential (TOF_0) confirming that **1**(H)$^+$ is indeed a better HER catalyst than **2**. DFT calculations further suggested that, owing to a strong structural rearrangement in the course of the catalytic cycle, the HER catalysis by the {2e$^–$,1H$^+$} intermediate of **1**(H)$^+$ only involves the iron center adjacent to the amine group in adt^H and not the two iron centers as in the corresponding {2e$^–$,1H$^+$} intermediate of **2**. This difference between the two catalytic mechanisms may explain the better of activity of **1.** As a matter of fact, it has been previously shown using phosphine-substituted diiron dithiolate complexes that terminal hydride species (FeFe–H) more easily undergo protonolyse to H_2 than their isomeric bridging hydride counterparts (Fe–H–Fe). This study provides a new example of the key role played by the nature of

the dithiolate bridging ligand on the mechanisms of electron and proton transfer in diiron complexes, and thus on their catalytic activities for the HER.

Acknowledgments

This work was supported by the Agence Nationale de la Recherche (ANR, BLANC SIMI9/0926-1, "TechBioPhyp »), the Centre National de la Recherche Scientifique (CNRS), and the Université de Bretagne Occidentale (UBO). We thank Prof. Rauchfuss at UIUC (USA) for the generous gift of $[Fe_2(adt^H)(CO)_6]$.

References

[1] W. Lubitz, H. Ogata, O. Rudiger, E. Reijerse, Hydrogenases, Chem. Rev. 114 (2014) 4081–4148. https://doi.org/10.1021/cr4005814.

[2] J.C. Fontecilla-Camps, A. Volbeda, C. Cavazza, Y. Nicolet, Structure/Function Relationships of [NiFe]- and [FeFe]-Hydrogenases, Chem. Rev. 107 (2007) 4273–4303. https://doi.org/10.1021/cr050195z.

[3] F. Gloaguen, T.B. Rauchfuss, Small molecule mimics of hydrogenases: hydrides and redox, Chem. Soc. Rev. 38 (2009) 100–108. https://doi.org/10.1039/b801796b.

[4] C. Tard, C.J. Pickett, Structural and Functional Analogues of the Active Sites of the [Fe]-, [NiFe]-, and [FeFe]-Hydrogenases, Chem. Rev. 109 (2009) 2245–2274. https://doi.org/10.1021/cr800542q.

[5] V. Artero, G. Berggren, M. Atta, G. Caserta, S. Roy, L. Pecqueur, M. Fontecave, From Enzyme Maturation to Synthetic Chemistry: The Case of Hydrogenases, Acc. Chem. Res. 48 (2015) 2380–2387. https://doi.org/10.1021/acs.accounts.5b00157.

[6] L. Sun, C. Duboc, K. Shen, Bioinspired Molecular Electrocatalysts for H2 Production: Chemical Strategies, ACS Catal. 12 (2022) 9159–9170. https://doi.org/10.1021/acscatal.2c02171.

[7] G. Hogarth, An unexpected leading role for [Fe2(CO)6(μ-pdt)] in our understanding of [FeFe]-H2ases and the search for clean hydrogen production, Coord. Chem. Rev. 490 (2023) 215174. https://doi.org/10.1016/j.ccr.2023.215174.

[8] T.B. Rauchfuss, Diiron Azadithiolates as Models for the [FeFe]-Hydrogenase Active Site and Paradigm for the Role of the Second Coordination Sphere, Acc. Chem. Res. 48 (2015) 2107–2116. https://doi.org/10.1021/acs.accounts.5b00177.

[9] M.E. Ahmed, A. Nayek, A. Križan, N. Coutard, A. Morozan, S. Ghosh Dey, R. Lomoth, L. Hammarström, V. Artero, A. Dey, A Bidirectional Bioinspired [FeFe]-Hydrogenase Model, J. Am. Chem. Soc. 144 (2022) 3614–3625. https://doi.org/10.1021/jacs.1c12605.

[10] M.L. Helm, M.P. Stewart, R.M. Bullock, M.R. DuBois, D.L. DuBois, A Synthetic Nickel Electrocatalyst with a Turnover Frequency Above 100,000 s-1 for H2 Production, Science. 333 (2011) 863–866. https://doi.org/10.1126/science.1205864.

[11] M.M. Roubelakis, D.K. Bediako, D.K. Dogutan, D.G. Nocera, Proton-coupled electron transfer kinetics for the hydrogen evolution reaction of hangman porphyrins, Energy Environ. Sci. 5 (2012) 7737–7740.

[12] R. Zaffaroni, N. Orth, I. Ivanović-Burmazović, J.N.H. Reek, Hydrogenase Mimics in M12L24 Nanospheres to Control Overpotential and Activity in Proton-Reduction Catalysis, Angew. Chem. 132 (2020) 18643–18647. https://doi.org/10.1002/ange.202008298.

[13] A. Dutta, A.M. Appel, W.J. Shaw, Designing electrochemically reversible H2 oxidation and production catalysts, Nat. Rev. Chem. 2 (2018) 244–252. https://doi.org/10.1038/s41570-018-0032-8.

[14] M. Bourrez, F. Gloaguen, Electrochemical and Computational Study of the Reactivity of a Diiron Azadithiolate Complex towards Protons in the Presence of Coordinating Anions, Eur. J. Inorg. Chem. 2015 (2015) 4986–4990. https://doi.org/10.1002/ejic.201500675.

[15] M. Bourrez, R. Steinmetz, F. Gloaguen, Mechanistic Insights into the Catalysis of Electrochemical Proton Reduction by a Diiron Azadithiolate Complex, Inorg. Chem. 53 (2014) 10667–10673. https://doi.org/10.1021/ic501815m.

[16] M. Bourrez, F. Gloaguen, Application of the energetic span model to the electrochemical catalysis of proton reduction by a diiron azadithiolate complex, New J. Chem. 39 (2015) 8073–8079. https://doi.org/10.1039/C5NJ00770D.

[17] A. Aster, S. Wang, M. Mirmohades, C. Esmieu, G. Berggren, L. Hammarström, R. Lomoth, Metal *vs.* ligand protonation and the alleged proton-shuttling role of the azadithiolate ligand in catalytic H_2 formation with FeFe hydrogenase model complexes, Chem. Sci. 10 (2019) 5582–5588. https://doi.org/10.1039/C9SC00876D.

[18] S.J. Borg, T. Behrsing, S.P. Best, M. Razavet, X. Liu, C.J. Pickett, Electron Transfer at a Dithiolate-Bridged Diiron Assembly: Electrocatalytic Hydrogen Evolution, J. Am. Chem. Soc. 126 (2004) 16988–16999. https://doi.org/10.1021/ja045281f.

[19] J.-F. Capon, S. Ezzaher, F. Gloaguen, F.Y. Pétillon, P. Schollhammer, J. Talarmin, Electrochemical Insights into the Mechanisms of Proton Reduction by [Fe2(CO)6{μ-SCH2N(R)CH2S}] Complexes Related to the [2Fe]H Subsite of [FeFe]Hydrogenase, Chem. - Eur. J. 14 (2008) 1954–1964. https://doi.org/10.1002/chem.200701454.

[20] E.S. Rountree, B.D. McCarthy, T.T. Eisenhart, J.L. Dempsey, Evaluation of Homogeneous Electrocatalysts by Cyclic Voltammetry, Inorg. Chem. 53 (2014) 9983–10002. https://doi.org/10.1021/ic500658x.

[21] C. Costentin, S. Drouet, M. Robert, J.-M. Savéant, Turnover Numbers, Turnover Frequencies, and Overpotential in Molecular Catalysis of Electrochemical Reactions. Cyclic Voltammetry and Preparative-Scale Electrolysis, J. Am. Chem. Soc. 134 (2012) 11235–11242. https://doi.org/10.1021/ja303560c.

[22] C. Costentin, J.-M. Savéant, Multielectron, Multistep Molecular Catalysis of Electrochemical Reactions: Benchmarking of Homogeneous Catalysts, ChemElectroChem. 1 (2014) 1226–1236.

https://doi.org/10.1002/celc.201300263.

[23] A. Molina, J. González, E. Laborda, Applicability of conventional protocols for benchmarking of unidirectional and bidirectional multi-electron homogeneous molecular catalysts beyond the pure kinetic regime, Electrochimica Acta. 428 (2022) 140934. https://doi.org/10.1016/j.electacta.2022.140934.

[24] V.C.-C. Wang, B.A. Johnson, Interpreting the Electrocatalytic Voltammetry of Homogeneous Catalysts by the Foot of the Wave Analysis and Its Wider Implications, ACS Catal. 9 (2019) 7109–7123. https://doi.org/10.1021/acscatal.9b00850.

[25] L.R. Almazahreh, F. Arrigoni, H. Abul-Futouh, M. El-khateeb, H. Görls, C. Elleouet, P. Schollhammer, L. Bertini, L. De Gioia, M. Rudolph, G. Zampella, W. Weigand, Proton Shuttle Mediated by (SCH2)2 P═O Moiety in [FeFe]-Hydrogenase Mimics: Electrochemical and DFT Studies, ACS Catal. 11 (2021) 7080–7098. https://doi.org/10.1021/acscatal.0c05563.

[26] S. Raugei, D.L. DuBois, R. Rousseau, S. Chen, M.-H. Ho, R.M. Bullock, M. Dupuis, Toward Molecular Catalysts by Computer, Acc. Chem. Res. (2015). https://doi.org/10.1021/ar500342g.

[27] D. Schilter, J.M. Camara, M.T. Huynh, S. Hammes-Schiffer, T.B. Rauchfuss, Hydrogenase Enzymes and Their Synthetic Models: The Role of Metal Hydrides, Chem. Rev. 116 (2016) 8693–8749. https://doi.org/10.1021/acs.chemrev.6b00180.

[28] F. Arrigoni, F. Rizza, J. Vertemara, R. Breglia, C. Greco, L. Bertini, G. Zampella, L. De Gioia, Rational Design of Fe2(μ-PR 2)2(L)6 Coordination Compounds Featuring Tailored Potential Inversion, ChemPhysChem. 21 (2020) 2279–2292. https://doi.org/10.1002/cphc.202000623.

[29] V. Fourmond, K. Hoke, H.A. Heering, C. Baffert, F. Leroux, P. Bertrand, C. Léger, SOAS: A free program to analyze electrochemical data and other one-dimensional signals, Bioelectrochemistry. 76 (2009) 141–147. https://doi.org/10.1016/j.bioelechem.2009.02.010.

[30] V. Fourmond, QSoas: A Versatile Software for Data Analysis, Anal. Chem. 88 (2016) 5050–5052. https://doi.org/10.1021/acs.analchem.6b00224.

[31] D.K. Gosser, Cyclic Voltammetry: Simulation and Analysis of Reaction Mechanisms, VCH, 1993.

[32] M.D. Hanwell, D.E. Curtis, D.C. Lonie, T. Vandermeersch, E. Zurek, G.R. Hutchison, Avogadro: an advanced semantic chemical editor, visualization, and analysis platform, J. Cheminformatics. 4 (2012) 17. https://doi.org/10.1186/1758-2946-4-17.

[33] F. Neese, F. Wennmohs, U. Becker, C. Riplinger, The ORCA quantum chemistry program package, J. Chem. Phys. 152 (2020) 224108. https://doi.org/10.1063/5.0004608.

[34] C. Lee, W. Yang, R.G. Parr, Development of the Colle-Salvetti correlation-energy formula into a functional of the electron density, Phys. Rev. B. 37 (1988) 785–789. https://doi.org/10.1103/PhysRevB.37.785.

[35] S. Grimme, S. Ehrlich, L. Goerigk, Effect of the damping function in dispersion corrected density functional theory, J. Comput. Chem. 32 (2011) 1456–1465.

https://doi.org/10.1002/jcc.21759.

[36] F. Weigend, R. Ahlrichs, Balanced basis sets of split valence, triple zeta valence and quadruple zeta valence quality for H to Rn: Design and assessment of accuracy, Phys. Chem. Chem. Phys. 7 (2005) 3297. https://doi.org/10.1039/b508541a.

[37] B. Helmich-Paris, B. de Souza, F. Neese, R. Izsák, An improved chain of spheres for exchange algorithm, J. Chem. Phys. 155 (2021) 104109. https://doi.org/10.1063/5.0058766.

[38] A.V. Marenich, C.J. Cramer, D.G. Truhlar, Universal Solvation Model Based on Solute Electron Density and on a Continuum Model of the Solvent Defined by the Bulk Dielectric Constant and Atomic Surface Tensions, J. Phys. Chem. B. 113 (2009) 6378–6396. https://doi.org/10.1021/jp810292n.

[39] J.A. Keith, K.A. Grice, C.P. Kubiak, E.A. Carter, Elucidation of the Selectivity of Proton-Dependent Electrocatalytic CO_2 Reduction by *fac* -Re(bpy)$(CO)_3$ Cl, J. Am. Chem. Soc. 135 (2013) 15823–15829. https://doi.org/10.1021/ja406456g.

[40] V.V. Pavlishchuk, A.W. Addison, Conversion constants for redox potentials measured versus different reference electrodes in acetonitrile solutions at 25°C, Inorganica Chim. Acta. 298 (2000) 97–102. https://doi.org/10.1016/S0020-1693(99)00407-7.

[41] C.Y. Legault, CYLView, (n.d.). https://www.cylview.org.

[42] T. Lu, F. Chen, Multiwfn: A multifunctional wavefunction analyzer, J. Comput. Chem. 33 (2012) 580–592. https://doi.org/10.1002/jcc.22885.

[43] R.G. Parr, W. Yang, Density functional approach to the frontier-electron theory of chemical reactivity, J. Am. Chem. Soc. 106 (1984) 4049–4050. https://doi.org/10.1021/ja00326a036.

[44] J.-F. Capon, S. Ezzaher, F. Gloaguen, F.Y. Pétillon, P. Schollhammer, J. Talarmin, T.J. Davin, J.E. McGrady, K.W. Muir, Electrochemical and theoretical investigations of the reduction of [Fe2(CO)5L{μ-SCH2XCH2S}] complexes related to [FeFe] hydrogenase, New J. Chem. 31 (2007) 2052. https://doi.org/10.1039/b709273c.

[45] A. Rana, P. Kumar Das, B. Mondal, S. Dey, D. Crouthers, A. Dey, Investigation of Bridgehead Effects on Reduction Potential in Alkyl and Aryl Azadithiolate-Bridged (μ-SCH2XCH2S) [Fe(CO)3]2 Synthetic Analogues of [FeFe]-H2ase Active Site, Eur. J. Inorg. Chem. 2018 (2018) 3633–3643. https://doi.org/10.1002/ejic.201800335.

[46] G.A.N. Felton, R.S. Glass, D.L. Lichtenberger, D.H. Evans, Iron-Only Hydrogenase Mimics. Thermodynamic Aspects of the Use of Electrochemistry to Evaluate Catalytic Efficiency for Hydrogen Generation, Inorg. Chem. 45 (2006) 9181–9184. https://doi.org/10.1021/ic060984e.

[47] P. Surawatanawong, J.W. Tye, M.Y. Darensbourg, M.B. Hall, Mechanism of electrocatalytic hydrogen production by a di-iron model of iron–iron hydrogenase: A density functional theory study of proton dissociation constants and electrode reduction potentials, Dalton Trans. 39 (2010) 3093. https://doi.org/10.1039/b925262b.

[48] C. Greco, G. Zampella, L. Bertini, M. Bruschi, P. Fantucci, L. De Gioia, Insights into the

Mechanism of Electrocatalytic Hydrogen Evolution Mediated by Fe2(S2C3H6)(CO)6 : The Simplest Functional Model of the Fe-Hydrogenase Active Site, Inorg. Chem. 46 (2007) 108–116. https://doi.org/10.1021/ic061168+.

[49] J.L. Stanley, Z.M. Heiden, T.B. Rauchfuss, S.R. Wilson, L. De Gioia, G. Zampella, Desymmetrized Diiron Azadithiolato Carbonyls: A Step Toward Modeling the Iron-Only Hydrogenases, Organometallics. 27 (2008) 119–125. https://doi.org/10.1021/om7009599.

Table 1. Experimental and calculated bond lengths (Å) and angles (°) in complex **1** (see text for the details of DFT calculations).

	Fe–Fe	Fe–S[(b)]	S–C[(b)]	Fe–S–Fe[(b)]	S–Fe–S[(b)]
Exp[(a)]	2.51	2.26	1.86	67.7	85.1
Calc	2.51	2.29	1.87	66.6	85.1

[(a)] see Ref.[49]. [(b)] average value.

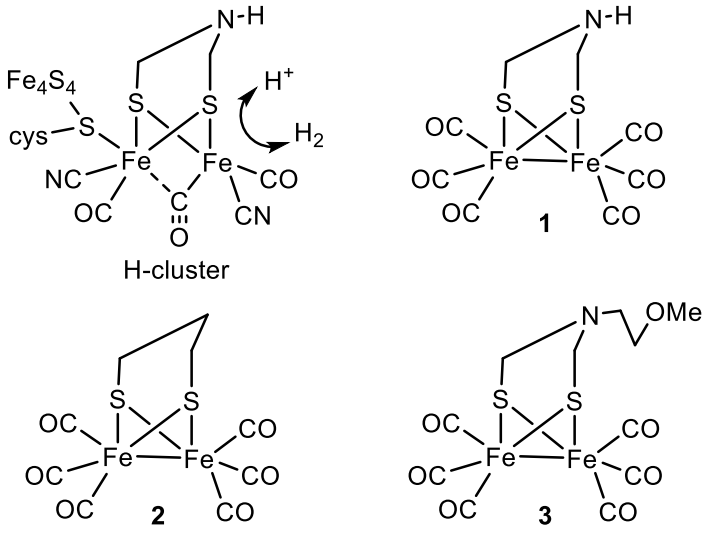

Scheme 1. Structures of the active site of [FeFe]-H_2ases (**H-cluster**), **1**, **2** and **3**.

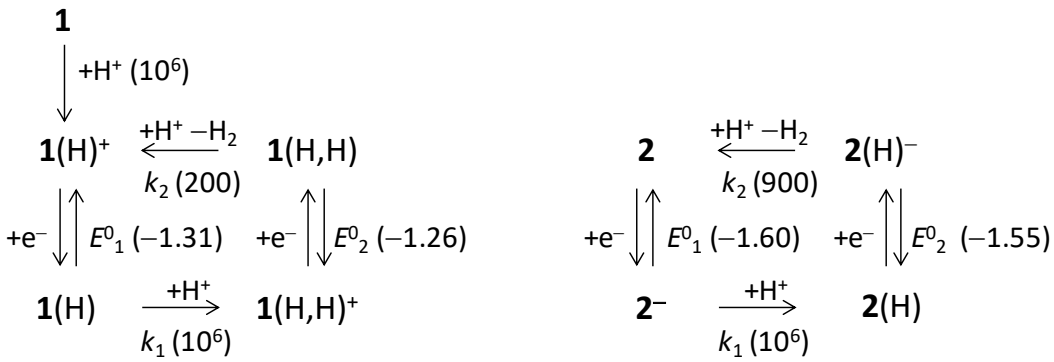

Scheme 2. (C)ECEC mechanism and parameter values (E^0 / V and k / M^{-1} s^{-1}) used to simulate the catalytic CV responses of **1**(H)$^+$ and **2** at low acid concentrations.

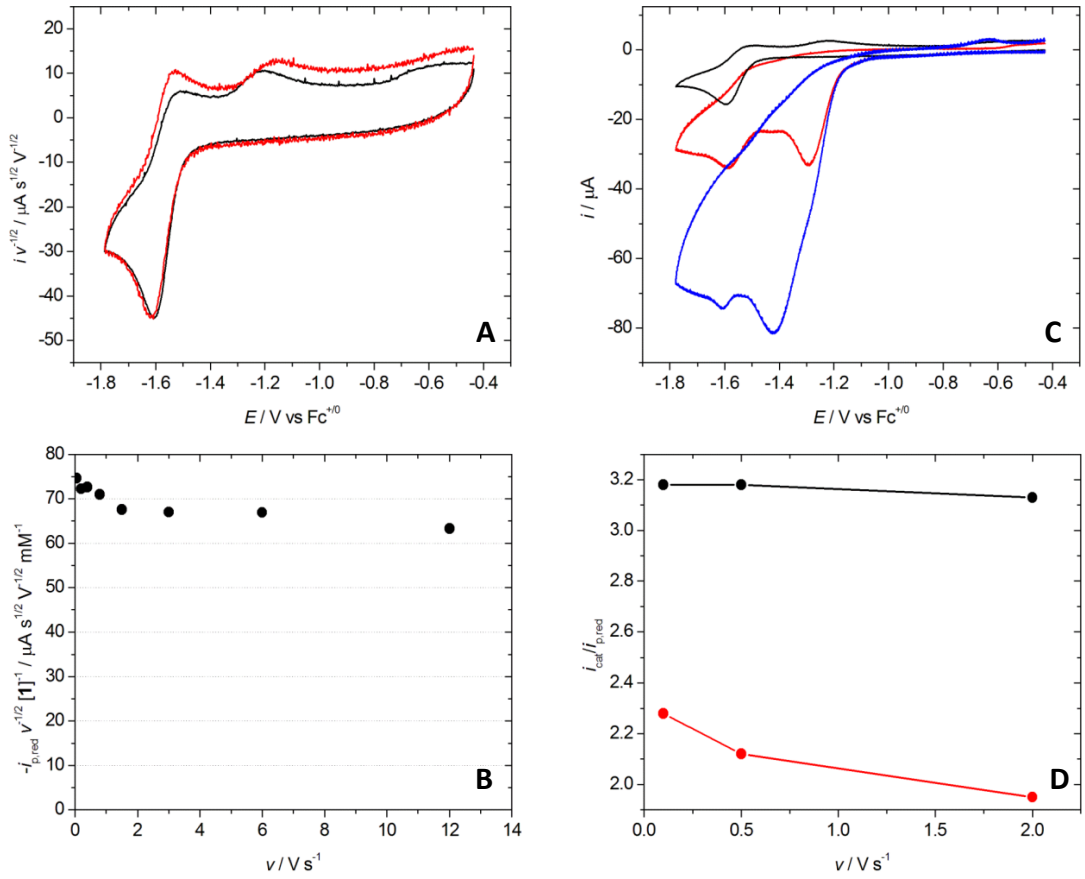

Fig. 1. A: normalized cyclic voltammograms of **1** (0.53 mM) in Bu_4NPF_6/MeCN recorded at scan rates v = 0.2 (black) and 0.8 V s^{-1} (red). **B**: plot of the normalized reduction peak current ($-i_{p,red}\ v^{-1/2}\ [\mathbf{1}]^{-1}$) as a function of the scan rate (v) showing no transition from one- to two electron-process. **C**: cyclic voltammograms of **1** (0.51 mM) recorded at 0.1 V s^{-1} in Bu_4NPF_6/MeCN in the presence of increasing concentrations of HOTs: 0 (black), 4 (red) and 12 (blue) molar equivalents. **D**: peak current enhancement $i_{cat}/i_{p,red}$ as a function of the scan rate v for **1** (red) and **2** (black) in the presence of 4 molar equivalents of HOTs.

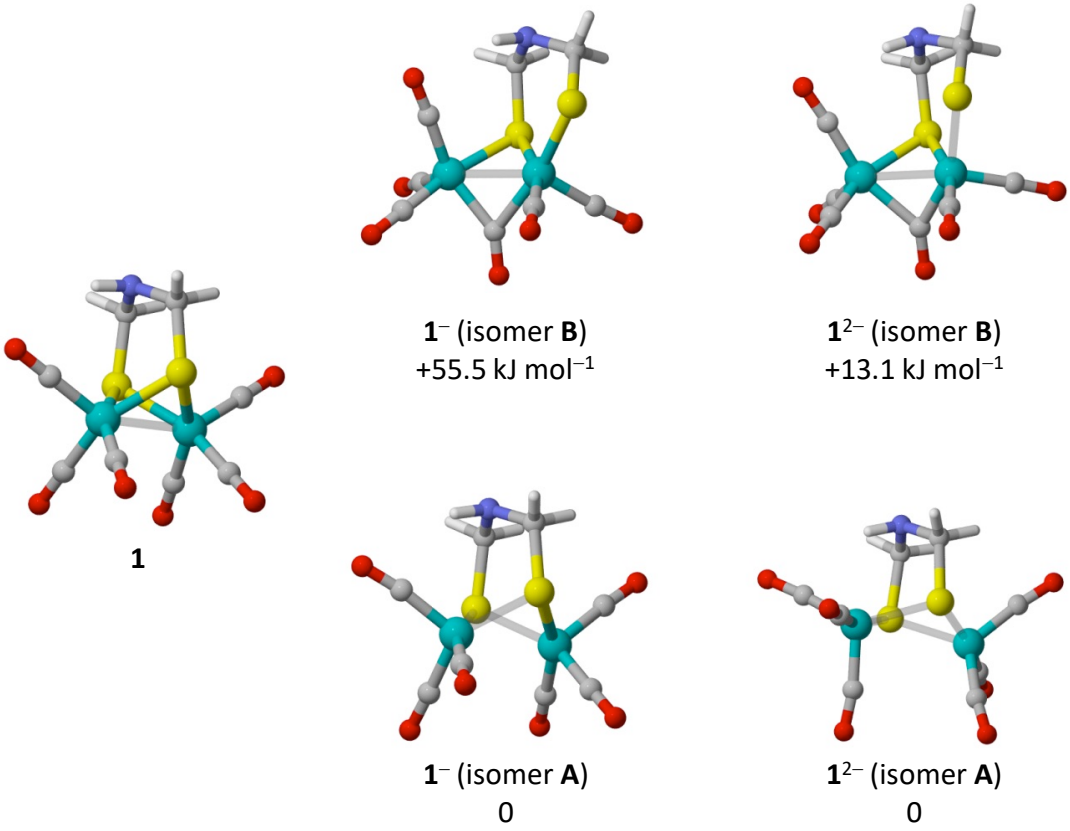

Fig. 2. Optimized geometries of **1**, $\mathbf{1}^{-}$ and $\mathbf{1}^{2-}$ and free energy differences (kJ mol^{-1}) between isomers **A** and **B**. Atom colors: Fe (green), S (yellow), C (grey), O (red), N (blue) and H (white).

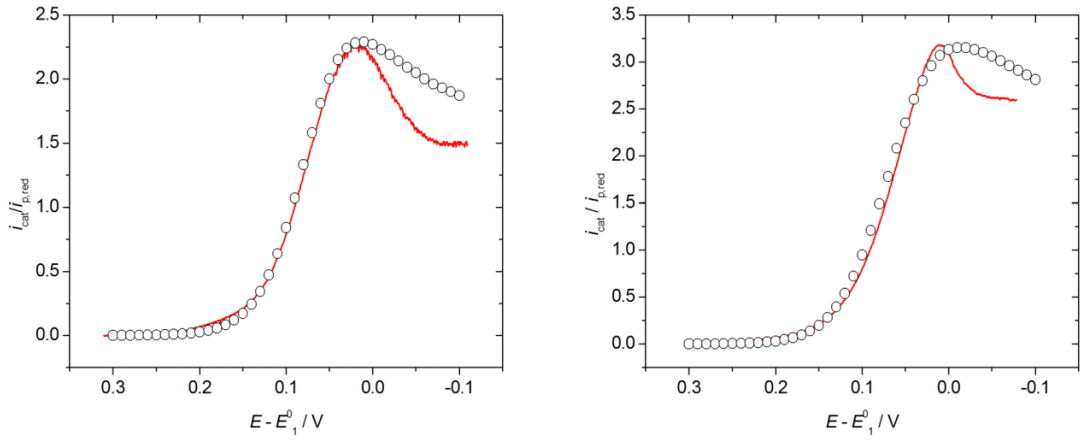

Fig. 3. Experimental (red trace) and simulated (open circle) catalytic CV responses of **1** (left) and **2** (right) at v = 0.1 V s^{-1} in the presence of 4 molar equivalents of HOTs. The experimental catalytic CV responses were corrected from background current and ohmic drop.

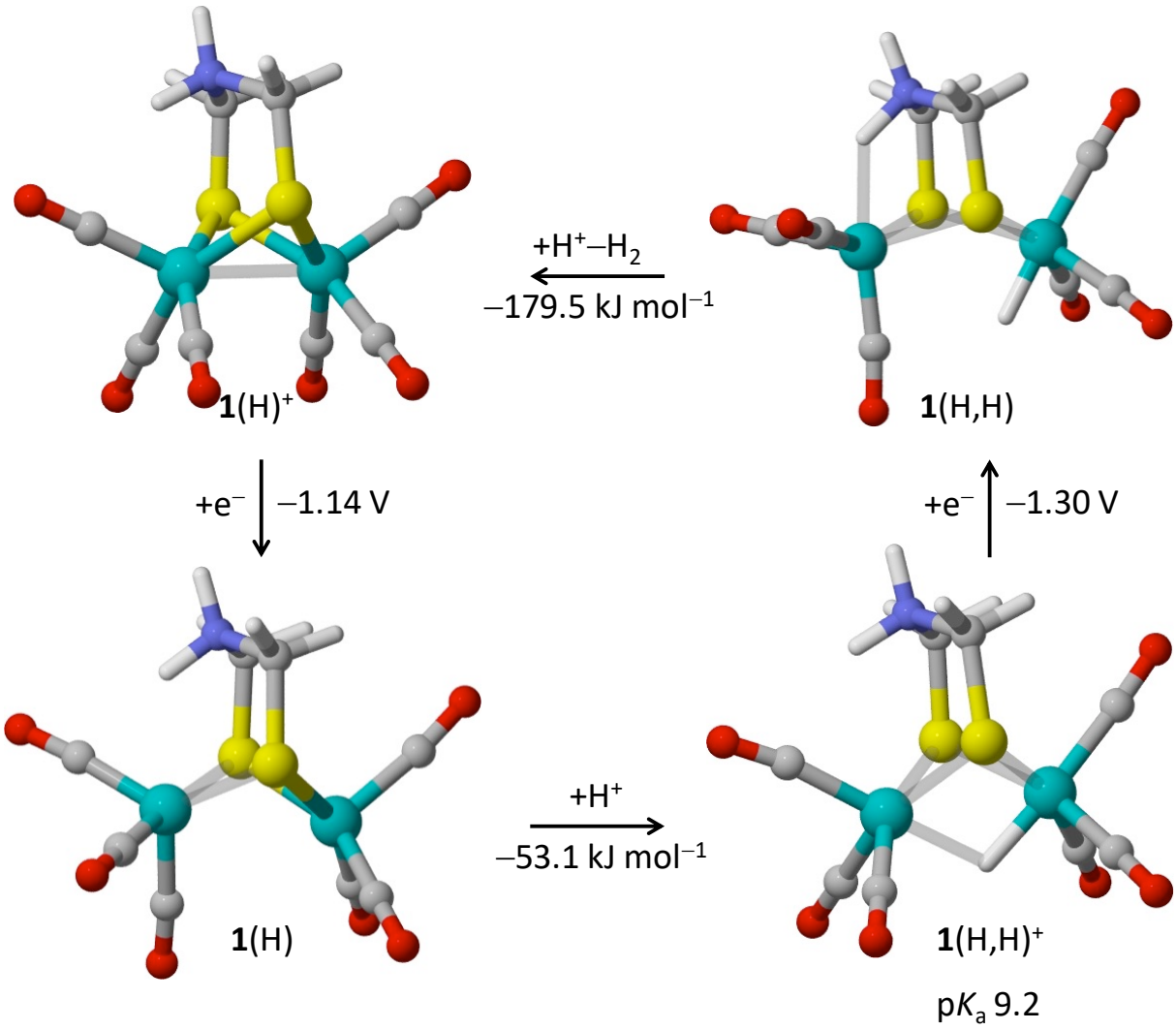

Fig. 4. Optimized geometries and calculated values of free energy of reaction (kJ mol^{-1}), standard potential (V) and pK_a of the intermediates involved in the HER catalysis by **1**(H)$^+$. Atom colors: Fe (green), S (yellow), C (grey), O (red), N (blue) and H (white).

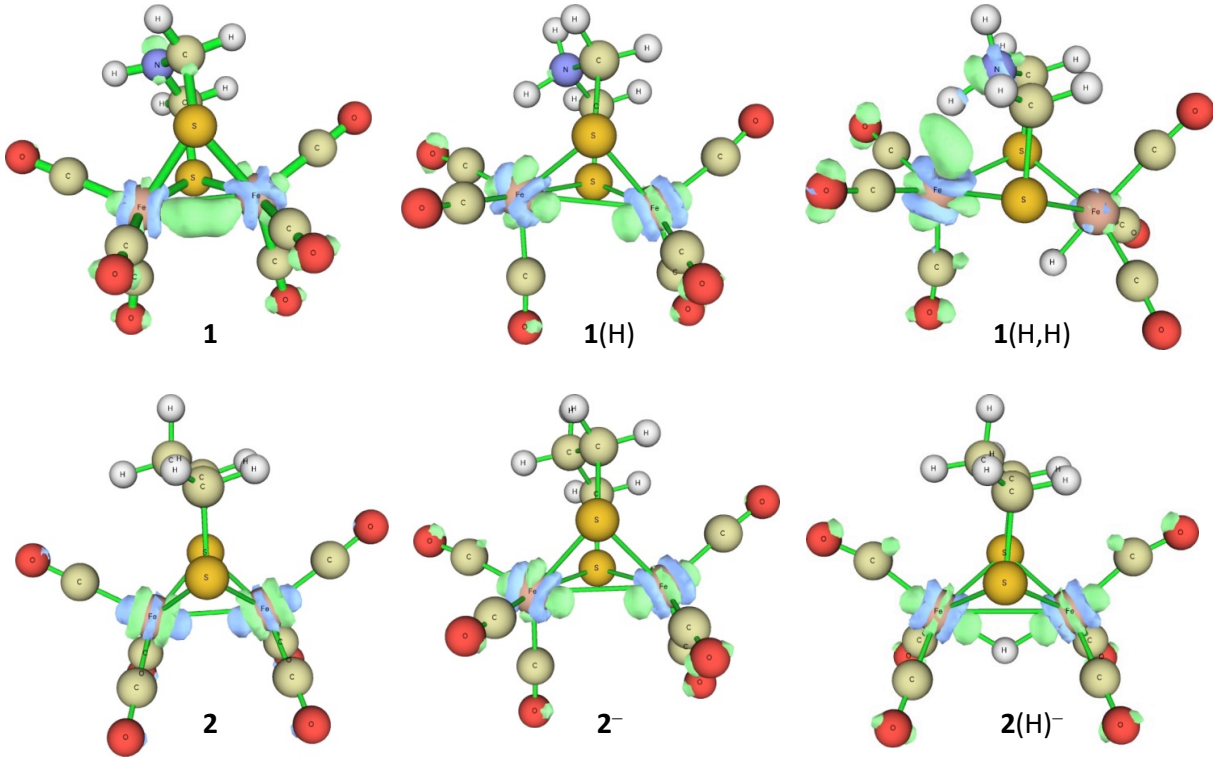

Fig. 5. Plots of the Fukui function revealing the reactive sites for an electrophilic attack (protonation) of the intermediate species involved in the HER catalysis by **1** and **2**. Green and blue isosurfaces (isovalue = 0.007) correspond to an increase and decrease of electron density, respectively.